This is the author's version of an article that has been published in this journal. Changes were made to this version by the publisher prior to publication. The final version is available at http://dx.doi.org/10.1109/TMTT.2016.2623902

Polynomial-Based Surrogate Modeling of RF and Microwave Circuits in Frequency Domain Exploiting the Multinomial Theorem

José L. Chávez-Hurtado and José E. Rayas-Sánchez

***Abstract*— A general formulation to develop EM-based polynomial surrogate models in frequency domain utilizing the multinomial theorem is presented in this paper. Our approach is especially suitable when the number of learning samples is very limited and no physics-based coarse model is available. We compare our methodology against other four surrogate modeling techniques: response surface modeling, support vector machines, generalized regression neural networks, and Kriging. Results confirm that our modeling approach has the best performance among these techniques when using a very small amount of learning base points on relatively small modeling regions. We illustrate our technique by developing a surrogate model for an SIW interconnect with transitions to microstrip lines, a dual band T-slot PIFA handset antenna, and a high-speed package interconnect. Examples are simulated on a commercially available 3D FEM simulator.**

***Index Terms*— EM-based design, FEM, multinomial theorem, package interconnect, PIFA antenna, polynomial surrogates, SIW interconnect, surrogate modeling.**

I. Introduction

Typically, direct optimization of microwave structures using full-wave electromagnetic (EM) simulators is computationally too expensive. A single EM simulation may take several hours, especially when using detailed physical models with high resolution discretization (fine EM model). Surrogate models can be exploited to accelerate the direct optimization process of high-frequency structures [1], [2], which additionally can be useful to hide the intellectual property of the EM design. In order to be useful for design optimization, surrogate models should be computationally cheap, smooth, and sufficiently accurate in the region of interest for the design parameters.

We can identify two types of surrogate models: physical and functional surrogates. A physical surrogate is usually implemented by a quasi-static approximation or an equivalent circuit; it can also be implemented in the same EM simulator used for the original structure under design, but using a coarse discretization [3] and removing some details of the original structure to speed up the simulation time [4]. However, these simplified and coarsely discretized full-wave EM models may exhibit numerical noise, discontinuous behavior, and non-negligible simulation time with respect to the corresponding original fine model [5].

On the other hand, functional surrogates, also called metamodels, are generated by using a set of learning base points from the original fine EM model. These learning base points are usually selected within a specified modeling region and can be allocated using design of experiments (DoE) techniques [3]. Functional surrogate approaches treat the EM model as a black box, with the goal to approximate the relationship between inputs and outputs of the structure under study [6].

Different approaches can be used to develop functional surrogate models for EM-based design. Among the most popular are: response surface methodology (RSM), artificial neural networks (ANN), support vector machines (SVM) and Kriging.

RSM uses a second-order polynomial to generate a surrogate model that represents the relationship between model inputs and outputs [7]-[9]. The number of unknowns in the second-order approximation defines the required number of function evaluations [7]. Some RSM techniques, such as the D-optimal DoE, require twice that number of function evaluations [10].

ANN can be seen as non-linear data modeling tools capable of representing complex relationships between model inputs and outputs [11], [12]. A multilayer ANN can approximate any input-output deterministic relationship by using a suitable amount of data and the correct number of hidden neurons [13]. Generally, the learning error hypersurface contains many local minima, making global optimization algorithms more desirable to train the ANN [14]. Additionally, the number of learning base points needed to approximate a function grows exponentially with the ratio between dimensionality and the degree of smoothness [13]. Generalized regression neural network (GRNN) is a special type of ANN that does not require an iterative training procedure [15]. The number of neurons in the hidden layer of a GRNN is equal to the number of learning samples. Some advantages of GRNN are fast learning and convergence to the optimal regression surface as the number of samples become very large, and no need of a minimum set of learning base points to train the neural network [16], [17]. Abundant examples of ANN-based surrogate modeling for microwave structures have been published, e.g., [13], [14], [18], [19].

SVM modeling solves a constrained quadratic optimization

This paper is an expanded version from the 2016 International Microwave Symposium, San Francisco, CA, May 22-27, 2016.

J. L. Chávez-Hurtado, and J. E. Rayas-Sánchez are with the Department of Electronics, Systems, and Informatics, ITESO – The Jesuit University of Guadalajara, Tlaquepaque, Jalisco, 45604 Mexico (phone +52 33 3669 3598; website: http://desi.iteso.mx/caecas; e-mail: erayas@iteso.mx). J. L. Chávez-Hurtado is funded through a CONACYT scholarship (*Consejo Nacional de Ciencia y Tecnología*, Mexican Government).

problem, allowing to find a global optimum for the model parameters. The optimization problem is feasible due to the utilization of a kernel function, including linear, polynomial, and radial basis functions. The radial basis function is the most employed kernel since it creates a nonlinear map, taking the samples into a higher dimensional space with less numerical difficulties to find an optimum solution [20], [21]. SVM models are trained by using the structural risk minimization principle, instead of the empirical risk minimization principle used by ANN models. The structural risk minimization principle allows SVM models to have a good trade-off between model complexity and generalization capability [22]. Since SVM models are based on small sample statistical learning theory, an optimum solution can be found by using a limited number of samples [21]. Examples of SVM modeling for microwave structures can be found in [23]-[26].

Kriging methodology exploits the best linear unbiased estimator (BLUE) of the output value for a given input to choose the weighting factors that minimize the prediction variance [27]. Implementation of RSM and ANN models usually employ classical DoE, where extreme scenarios are commonly simulated, such as the corners of the corresponding modeling region. However, Kriging methodology is based on space-filling experiments, usually implemented by using the Latin hypercube design (LHD) [27]. Kriging models aim at covering the whole experimental area, consequently, they can be seen as a global metamodels [28]. If there are not enough function evaluations of the EM model, the Kriging estimated correlation function tends to be noisy and the predictions become inaccurate [27]. Different Kriging techniques have been developed, such as simple Kriging, ordinary Kriging, universal Kriging, Taylor Kriging, and dynamic Kriging [29]. Examples of Kriging surrogate modeling of microwave structures can be found in [30], [31]

The surrogate modeling methodology proposed in this work exploits the multinomial theorem to represent the relationship between model inputs and outputs by using polynomial functions at each simulated frequency point. Corresponding surrogate model weighting factors are calculated in closed form by using frugal learning base point distributions (e.g., star or box distribution), achieving a global minimum in the least squares sense. In contrast to RSM, the order of the polynomial function is not fixed and can be increased until generalization performance deteriorates.

A similar approach to develop polynomial surrogate models is proposed in [32]; however, our new approach differs in three aspects: the surrogate model formulation, the calculation of weighting factors, and the surrogate order determination. For the surrogate model formulation, [32] implements the *N*th order surrogate model by using an element-wise power operator, which creates some redundant terms, while our new formulation exploits the multinomial theorem, allowing us to expand a polynomial raised to an arbitrary power including all cross terms and no redundant terms. For the weighting factors calculation, the approach in [32] calculates simultaneously all weighting factors available for each surrogate model order. In contrast, the proposed approach in this work automatically calculates the weighting factors by assuming that lower-order surrogates are fixed or by calculating all weighting factors simultaneously, and the selection between both manners is based on the conditional number of the system matrix. Finally, the order of the surrogate model can be different for each simulated frequency point, while in [32] and [33] the same surrogate model order is used for all simulated frequency points.

The present article expands our work in [34] by: a) presenting the general formulation for the *N*th-order surrogate model; b) comparing and discussing the number of weighting factors required by the proposed new polynomial-based surrogate modeling (PSM) methodology versus the polynomial formulation presented in [32]; c) developing two additional surrogate modeling examples: a single-layer substrate integrated waveguide (SIW) interconnect with transitions to microstrip lines and a high-speed package interconnect; d) comparing at some testing base points the actual EM responses of the original fine model and the corresponding PSM model responses; and e) presenting and discussing the performance of our PSM proposal when varying the size of the region of interest, as well as some potential applications.

The organization of this paper is as follows: Section II describes the general PSM formulation. Section III presents the PSM training, including the selection of the polynomials order. Section IV shows the performance of our proposal for three surrogate modeling examples, comparing it versus other approaches. Section V elaborates on the modeling region size and potential applications. Finally, Section VI concludes this work.

II. General PSM Formulation

Let $\boldsymbol{R}_\mathrm{f} \in \Re^p$ denote a fine model response sampled at p frequency points. We assume that $\boldsymbol{R}_\mathrm{f}$ only depends on the design variables $\boldsymbol{x} \in \Re^n$. We treat the fine model as a multidimensional vector function, $\boldsymbol{R}_\mathrm{f}(\boldsymbol{x}) : X_\mathrm{f} \rightarrow \Re^p$ whose domain is $X_\mathrm{f} \subseteq \Re^n$. We aim to develop a surrogate model $\boldsymbol{R}_\mathrm{s}(\boldsymbol{x})$: $X_\mathrm{s} \rightarrow \Re^p$ that approximates $\boldsymbol{R}_\mathrm{f}(\boldsymbol{x})$ in a region of interest $X_\mathrm{s} \subseteq X_\mathrm{f}$, around the reference design $\boldsymbol{x}^{(0)}$, where $\boldsymbol{\Delta x} \in \Re^n$ is the distance from a given design to that reference, $\boldsymbol{\Delta x} = \boldsymbol{x} - \boldsymbol{x}^{(0)}$.

A. Nth-order Surrogate Model

A general expression for an *N*th-order surrogate model at the *k*-th simulated frequency point can be written as

$$R_{sk}^{(N)}(\boldsymbol{x}) = R_{sk}^{(N-1)}(\boldsymbol{x}) + \boldsymbol{w}_k^{(N)\mathrm{T}} \boldsymbol{q}^{(N)}(\boldsymbol{\Delta x}) \quad (1),$$

where $\boldsymbol{w}_k^{(N)} \in \Re^{(N+n-1)!/((n-1)!(N)!)}$ has the weighting factors and $\boldsymbol{q}^{(N)}(\boldsymbol{\Delta x}) \in \Re^{(N+n-1)!/(n-1)!(N)!}$ the multinomial terms for $\boldsymbol{\Delta x}$. The scalar elements of $\boldsymbol{q}^{(N)}$ are given by

$$q^{(N)}(\boldsymbol{\Delta x}) = \Delta x_{\lambda_1} \Delta x_{\lambda_2} \cdots \Delta x_{\lambda_N} \quad (2),$$

for $\lambda_1 = 1{:}n$, $\lambda_2 = \lambda_1{:}n$, …, $\lambda_N = \lambda_{N-1}{:}n$.'

The zero-order model response is equal to $\boldsymbol{R}_\mathrm{f}(\boldsymbol{x}^{(0)})$ at all frequency points, as described in [34]. The first-order surrogate model is formulated by including weighting factors $\boldsymbol{w}_k^{(1)}$ and multinomial terms $\boldsymbol{q}^{(1)}$. The second-order surrogate model is formulated by incorporating the second-order terms $\boldsymbol{w}_k^{(2)}$ and $\boldsymbol{q}^{(2)}$, etc. See [34] for more details.

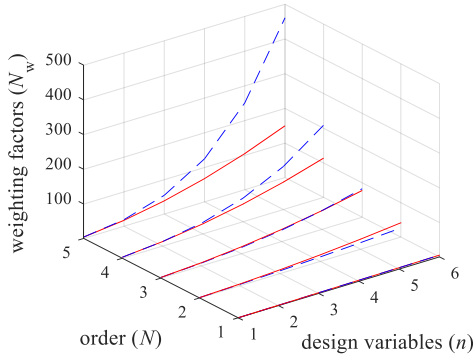

Fig. 1. Comparison in terms of total number of weighting factors for both polynomial surrogate formulations: a) old formulation [32] (solid line) and b) new formulation (dashed line).

B. Comparing Polynomial Surrogate Model Structures

The total number of weighting factors, N_w, used by the N-th order polynomial surrogate model employed in [32] is

$$N_w = (N-1)n^2 + n \quad (3).$$

On the other hand, our new polynomial surrogate model uses

$$N_w = n + \frac{n(n+1)}{2!} + \frac{n(n+1)(n+2)}{3!} + \ldots + \frac{(N+n-1)!}{N!(n-1)!} \quad (4).$$

A comparison between both formulations in terms of the total number of weighting factors is realized in Fig. 1. Both formulations use the same number of weighting factors in the following cases: a) when $N = 1$, for any n; b) when $n = 1$, for any N, c) when $N = 3$, for $n = 5$; and d) when $N = 4$, for $n = 2$. The new formulation uses a smaller number of weighting factors in two cases: a) when $N = 2$, for any n; and b) when $N = 3$, for $n \leq 4$. Moreover, since our new formulation does not incorporate redundant terms, the generalization performance is expected to be better than in [32], at least in all the previously mentioned cases, as it was experimentally confirmed in [33].

III. PSM Training

"Training" the surrogate models formulated in the previous section is done by calculating in closed form the corresponding weighting factors. We define a region of interest X_s delimited by a vector $\boldsymbol{\tau} \in \Re^n$ containing the relative deviations for each design variable with respect to $\boldsymbol{x}^{(0)}$. The corresponding weighting factors are calculated in closed form by using L learning base points within X_s, denoted as $\boldsymbol{x}^{(1)}$, $\boldsymbol{x}^{(2)}$, …, $\boldsymbol{x}^{(L)}$. The generalization performance is measured by using T testing base points within the same region. Weighting factors can be calculated in two different forms: a) by reusing lower-order weights and calculating only current-order weights, or, b) by calculating all weights simultaneously for each surrogate model order.

A. Weighting Factors Calculation Reusing Weights

Considering that the lower-order weights are already calculated and fixed, the fine model and the Nth-order surrogate model are matched at the j-th learning base point,

$$R_{fk}(\boldsymbol{x}^{(j)}) = R_{sk}^{(N-1)}(\boldsymbol{x}^{(j)}) + \boldsymbol{w}_k^{(N)\mathrm{T}}\boldsymbol{q}^{(N)}(\boldsymbol{\Delta x}^{(j)}) \quad (5),$$

for $j = 1, \ldots, L$. The Nth-order weights are then calculated by solving for $\boldsymbol{w}_k^{(N)}$ the following system of linear equations

$$\boldsymbol{Q}^{(N)}\boldsymbol{w}_k^{(N)} = \boldsymbol{\Delta R}_k^{(N)} \text{ for } k = 1, \ldots, p \quad (6),$$

with $\boldsymbol{Q}^{(N)} \in \Re^{(N+n-1)!/((n-1)!(N)!)}$ and $\boldsymbol{\Delta R}_k^{(N)} \in \Re^L$ defined as

$$\boldsymbol{Q}^{(N)} = \begin{bmatrix} \boldsymbol{q}^{(N)}(\boldsymbol{\Delta x}^{(1)})^{\mathrm{T}} \\ \boldsymbol{q}^{(N)}(\boldsymbol{\Delta x}^{(2)})^{\mathrm{T}} \\ \vdots \\ \boldsymbol{q}^{(N)}(\boldsymbol{\Delta x}^{(L)})^{\mathrm{T}} \end{bmatrix} \quad (7),$$

$$\boldsymbol{\Delta R}_k^{(N)} = \begin{bmatrix} R_{fk}(\boldsymbol{x}^{(1)}) - R_{sk}^{(N-1)}(\boldsymbol{x}^{(1)}) \\ \vdots \\ R_{fk}(\boldsymbol{x}^{(L)}) - R_{sk}^{(N-1)}(\boldsymbol{x}^{(L)}) \end{bmatrix} \quad (8).$$

B. Calculating All Weighting Factors Simultaneously for Each Surrogate Model Order

Consider now that all the weighting factors are simultaneously calculated at each surrogate model order. The corresponding responses of the fine model and the Nth-order surrogate model are matched at the j-th learning base point,

$$R_{fk}(\boldsymbol{x}^{(j)}) = R_{sk}^{(0)}(\boldsymbol{x}^{(j)}) + \boldsymbol{w}_k^{(1)}\boldsymbol{q}^{(1)\mathrm{T}}(\boldsymbol{\Delta x}^{(j)}) + \ldots + \boldsymbol{w}_k^{(N)}\boldsymbol{q}^{(N)\mathrm{T}}(\boldsymbol{\Delta x}^{(j)}) \quad (9),$$

for $j = 1, \ldots, L$. Weighting factors are then calculated by solving for $\boldsymbol{W}^{(N)}$ the following system of linear equations

$$\boldsymbol{Q}_{\mathrm{All}}^{(N)}\boldsymbol{W}^{(N)} = \boldsymbol{\Delta R}_k \text{ for } k = 1, \ldots, p \quad (10),$$

with $\boldsymbol{Q}^{(N)}{}_{\mathrm{ALL}} \in \Re^{L \times C}$, $\boldsymbol{W}^{(N)} \in \Re^{L \times C}$ and C defined as

$$\boldsymbol{Q}_{\mathrm{All}}^{(N)} = \begin{bmatrix} \boldsymbol{Q}^{(1)} & \boldsymbol{Q}^{(2)} & \cdots & \boldsymbol{Q}^{(N)} \end{bmatrix} \quad (11),$$

$$\boldsymbol{W}^{(N)} = \begin{bmatrix} \boldsymbol{w}_k^{(1)} & \boldsymbol{w}_k^{(2)} & \cdots & \boldsymbol{w}_k^{(N)} \end{bmatrix} \quad (12),$$

$$C = \sum_1^N \frac{(N+n-1)!}{(n-1)!(N)!} \quad (13).$$

C. Selecting Weighting Factors Calculation

The selection between the both previously defined forms to calculate the weighting terms is automatically realized in our surrogate modeling algorithm by comparing the condition number of matrices $\boldsymbol{Q}^{(N)}$ in (6) and $\boldsymbol{Q}^{(N)}{}_{\mathrm{ALL}}$ in (10). If the condition number of matrix $\boldsymbol{Q}^{(N)}$ is smaller than the condition number of matrix $\boldsymbol{Q}^{(N)}{}_{\mathrm{ALL}}$, weighting factors are calculated by solving (6), otherwise, by solving (10). This test is inexpensive, since no fine model evaluations are implied. In summary, we solve the best conditioned system of linear equations between (6) and (10), which only depends on the input learning base points and the order of the current polynomial surrogate.

D. Setting the Order of the Polynomial Function

As mentioned before, a polynomial function is developed at each simulated frequency point. The order of that polynomial is increased until generalization error deteriorates. This allows us to use a different polynomial order at each simulated frequency point, depending on the behavior, within the region of interest, of the EM response of the structure under study.

IV. Examples

For developing the surrogate models in all the following

examples, we employ a small amount of learning base points by using star and box distributions. The resultant number of base points are $2n$ and 2^n, respectively. For reliable assessment of the generalization performance we use K^n testing base points uniformly distributed, where K corresponds to the number of points for each design parameter.

For all the examples, we calculate the maximum absolute error in all the learning base points at each simulated frequency point, denoted as ϵ_L, as well as the maximum absolute error in all the testing base points at each simulated frequency point, denoted as ϵ_T. Since both errors, ϵ_L and ϵ_T, are calculated from S-parameters, they are dimensionless. To denote the largest maximum absolute error in the complete frequency sweep we use ϵ_{Lmax} and ϵ_{Tmax}, for the learning and testing sets, respectively.

The corresponding polynomial-based surrogate model performance for each example is compared with other four functional surrogate modeling techniques: RSM, SVM, Kriging and GRNN. SVM, Kriging and GRNN are implemented using the corresponding Matlab Toolboxes with the default settings.

In all the following examples, we perform the EM simulations using a conventional laptop (core i5 CPU with 8 GB RAM).

A. SIW Interconnect with Transitions to Microstrip Lines

Consider the SIW interconnect with transitions to microstrip lines proposed in [32], whose geometry is shown in Fig. 2. The purpose of the tapered microstrip transitions is to perform field conversion and impedance matching of the two dissimilar guiding structures [35].

1) Design Parameters

The SIW is designed on a substrate with a relative permittivity $\varepsilon_r = 3.6$ and a thickness $H = 0.4064$ mm. The SIW interconnect has a length $L_{SIW} = 4W$ and an external width $W = 9.6446$ mm. According to the required cutoff frequency for the dominant mode $f_{c10} = 10$ GHz, the internal width of the SIW interconnect is $W_{SIW} = 8.6845$ mm [32]. Vias have a diameter $d = 0.4801$ mm and are separated from their neighboring via by a center-to-center spacing $s = 2d$. The microstrip lines have a width $W_p = 0.8672$ mm and a length $L_p = 1.5W$. The transition uses $L_{tap} = 3W_{SIW}$ and $W_{tap} = (W_{SIW} + W_p)/2$.

Our model, implemented in COMSOL, neglects dielectric and metallic losses. Lateral and upper walls of the simulation bounding box are configured as scattering boundary condition. We follow a meshing scheme by zones as proposed in [36] and the bounding box dimensions proposed in [37]. We use a fine resolution discretization. Each frequency sweep takes around 1 h 20 min.

2) Surrogate Model Implementation

We develop a polynomial surrogate model for $|S_{21}|$ as a function of $\boldsymbol{x} = [W_{tap} \;\; L_{tap}]^T$ (see Fig. 2), using as a reference design $\boldsymbol{x}^{(0)} = [(W_{SIW}+W_p)/2 \;\; 3W_{SIW}]^T$, over a region defined by $\boldsymbol{\tau} = \pm [5\% \;\; 5\%]^T$. EM response of the SIW interconnect at $\boldsymbol{x}^{(0)}$ is shown in Fig. 3. To measure the generalization performance of the resultant polynomial surrogate we use a uniform distribution with $K = 4$ (resulting 16 testing base points).

The maximum absolute testing errors as well as the order of the polynomial implemented at each simulated frequency point, for both learning base point distributions, are shown in Fig. 4. Notice that there are some frequency points where the polynomial reaches the 10^{th} order. This is due to the high nonlinearity of the EM responses, within the modeling region, at those frequency points.

EM responses of the surrogate model at some testing base

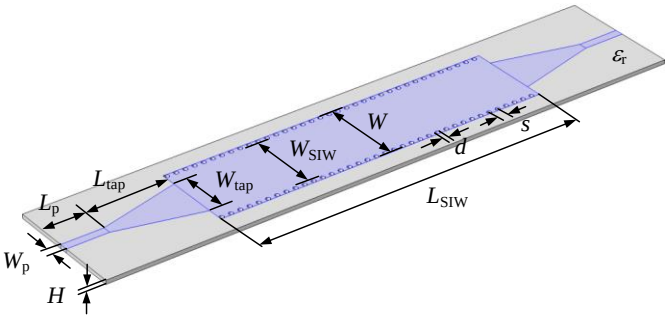

Fig. 2. Single-layer substrate integrated waveguide (SIW) interconnect with microstrip transitions. From [32].

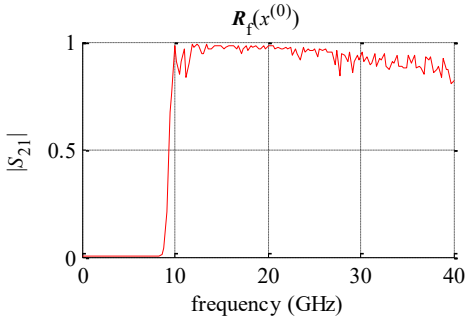

Fig. 3. EM response of the SIW interconnect with microstrip transitions at $\boldsymbol{x}^{(0)}$. From [32].

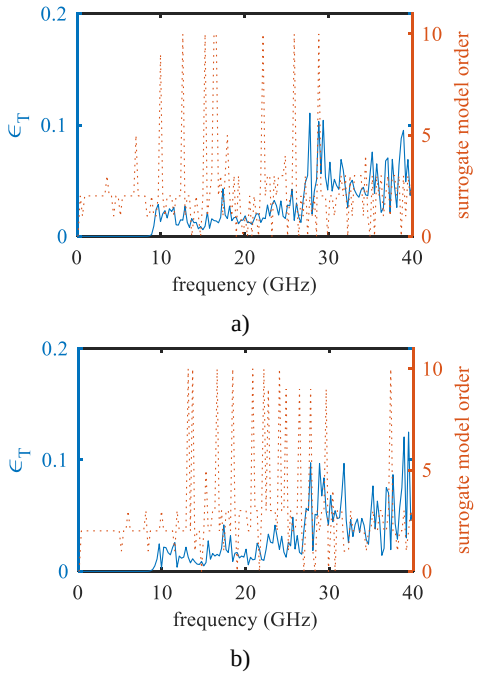

Fig. 4. Surrogate model maximum absolute testing error (solid line) and polynomial order (dotted line), at each frequency point, for the SIW example, using: a) a star distribution; b) a box distribution of learning base points.

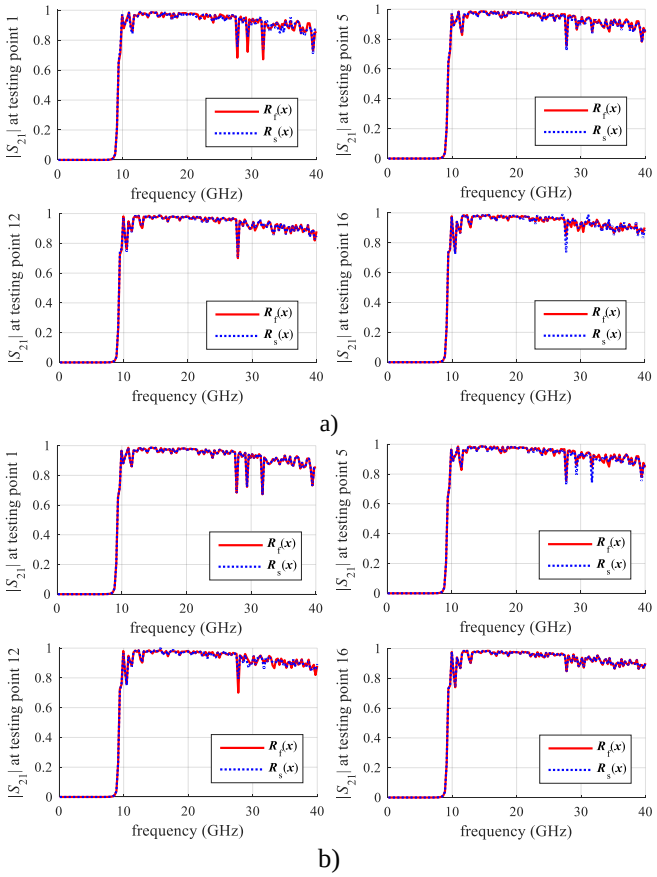

Fig. 5. Comparison between EM model and polynomial surrogate model responses at some testing base points, for the SIW example. Polynomial surrogate obtained from: a) a star distribution; and b) a box distribution of learning base points.

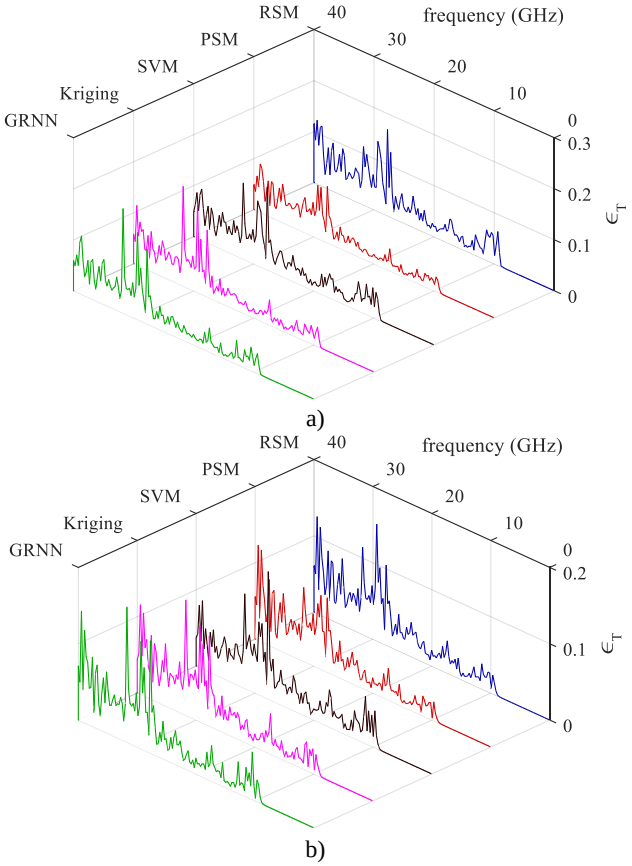

Fig. 6. Maximum testing errors for $|S_{21}|$ of the SIW interconnect using a uniform testing base point distribution with $K = 4$ and using: a) a star distribution of learning base points ($2n = 4$); b) a box distribution of learning base points ($2^n = 4$).

points, with polynomial surrogates trained with both learning base point distributions, are shown in Fig. 5. We can see there is a very good match between the fine and the surrogate model responses at the testing base points.

3) Performance Comparison

Using the same learning and testing base point distributions, the corresponding maximum absolute testing errors at each simulated frequency point, for the five implemented surrogate models, are shown in Fig. 6. Numerically, Table I shows the largest maximum absolute learning and testing errors for each implemented surrogate model. These results show that the proposed polynomial-based surrogate model achieves the best generalization performance with both learning base point distributions.

TABLE I
SIW INTERCONNECT SURROGATE MODELS PERFORMANCE FOR $|S_{21}|$

model	star distribution		box distribution	
	ϵ_{Tmax}	ϵ_{Lmax}	ϵ_{Tmax}	ϵ_{Lmax}
RSM	0.16921	1.93e-14	0.15296	8.44e-15
PSM	0.11067	0.08567	0.12502	0.096922
SVM	0.16160	0.14324	0.16686	0.083662
Kriging	0.19523	0.12441	0.15086	0.150860
GRNN	0.20462	0	0.17695	0

B. Dual-Band Planar Inverted F Handset Antenna with Slotted Ground

For the second example, consider the T-slot planar inverted F handset (PIFA) antenna proposed in [38]. Its geometry is shown in Fig. 7. The bandwidth is increased by removing two portions of the metallization at the ground plane. The antenna design is intended to operate at the following bands: GSM900 (880-960 MHz), GSM1900 (1850-1990 MHz), UMTS2100 and WCDMA2100 (1920-2170 MHz).

1) Design Parameters

The PIFA is implemented on a substrate with a relative permittivity $\varepsilon_r = 2.2$, a dielectric loss tangent $\tan(\delta) = 0.009$ and a thickness $H = 3.962$ mm. The design parameters values are defined as $W_1 = 3.83$ mm, $W_2 = 8.85$ mm, $W_3 = 11$ mm, $W_4 = 1.54$ mm, $L_1 = 8.10$ mm, $L_2 = 20.34$ mm, $L_p = 24$ mm, $Y_f = 14$ mm, $X_f = 19.16$ mm, $Y_g = 18.9$ mm and, $X_g = 1$ mm.

The structure is implemented in COMSOL by using the simulation bounding box dimensions, boundary conditions, and the meshing scheme proposed in [38]. All metals are defined as perfect electric conductors. We use a relatively coarse resolution discretization, such that each frequency sweep takes around 2 min 20 s.

2) Surrogate Model Implementation

To develop the surrogate model, we define as design variables the parameters $\boldsymbol{x} = [W_1 \quad W_2 \quad L_1 \quad L_2]^T$, using as a reference design $\boldsymbol{x}^{(0)} = [3.83 \quad 8.85 \quad 8.10 \quad 20.34]^T$ (mm), over a region defined by $\boldsymbol{\tau} = \pm [5\% \quad 5\% \quad 5\% \quad 5\%]^T$. The EM response of the antenna at $\boldsymbol{x}^{(0)}$ is illustrated in Fig. 8. To

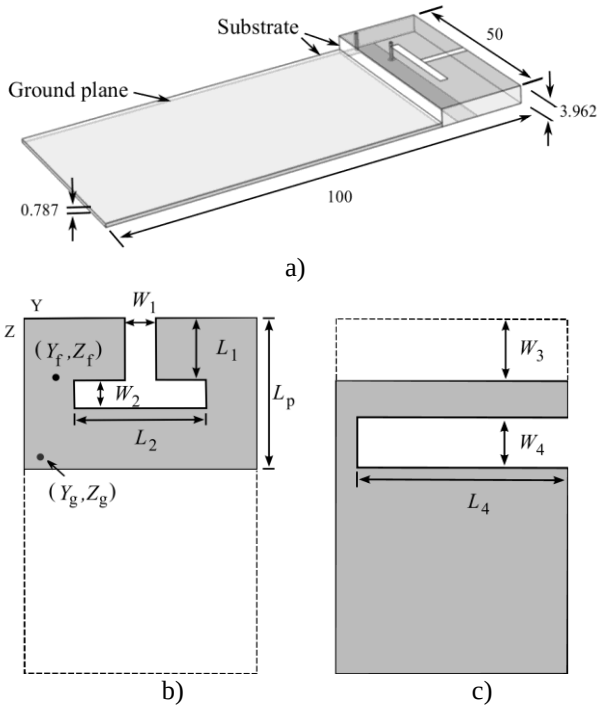

Fig. 7. T-slot dual band PIFA handset antenna: a) 3D view, b) top view, c) bottom view. From [38].

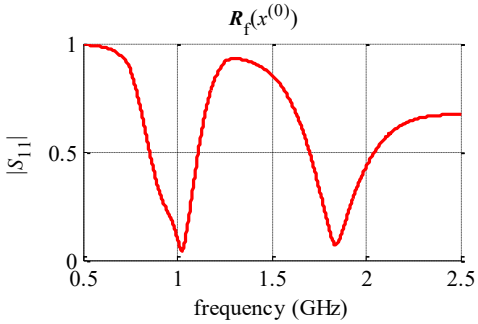

Fig. 8. EM response of the T-slot dual band PIFA antenna at the reference design $\boldsymbol{x}^{(0)}$. From [38].

measure the generalization performance of the resultant surrogate model we use a uniform distribution of testing base points with $K = 3$ (resulting 81 testing base points).

For both learning base point distributions, the maximum absolute testing errors as well as the order of the polynomial implemented at each simulated frequency points are shown in Fig. 9. Notice that, for the star distribution, a polynomial order higher than 2 is not required, while for the box distribution, a polynomial order higher than 4 is not required.

EM responses of the surrogate model at some testing base points, with polynomial surrogates trained with both learning base point distributions, are shown in Fig. 10. It is seen that there is an excellent match between the fine and the surrogate model responses at the testing base points.

3) Performance Comparison

Using the same learning and testing base point distributions, the corresponding maximum absolute testing errors at each simulated frequency point, for the five implemented surrogate models, are shown in Fig. 11. Numerically, Table II shows the largest maximum absolute learning and testing errors for the

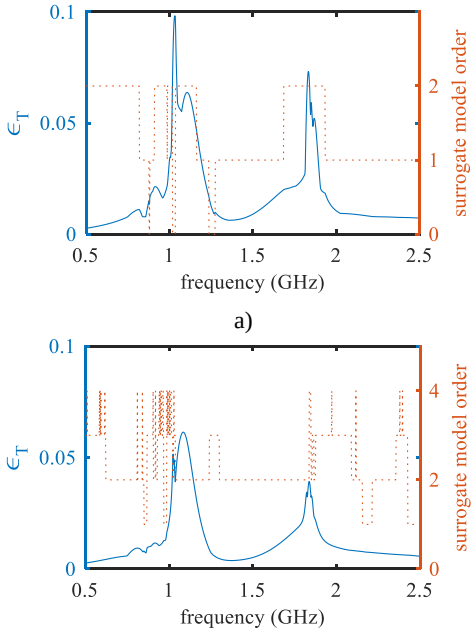

Fig. 9. Surrogate model maximum absolute testing error (solid line) and polynomial order (dotted line), at each frequency point, for the PIFA example, using: a) a star distribution; b) a box distribution of learning base points.

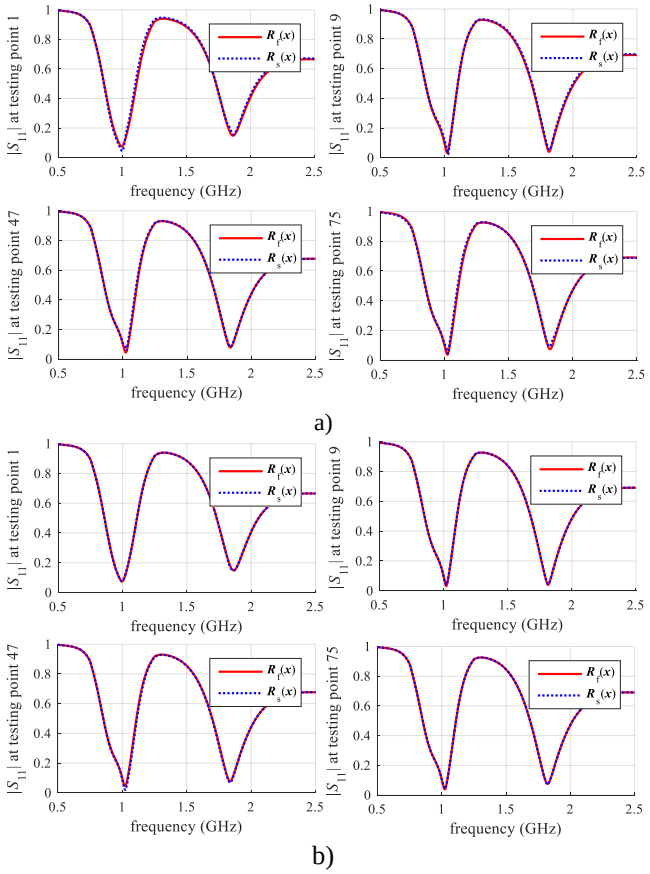

Fig. 10. Comparison between EM model and polynomial surrogate model responses at some testing base points, for the PIFA example. Polynomial surrogate obtained from: a) a star distribution; and b) a box distribution of learning base points.

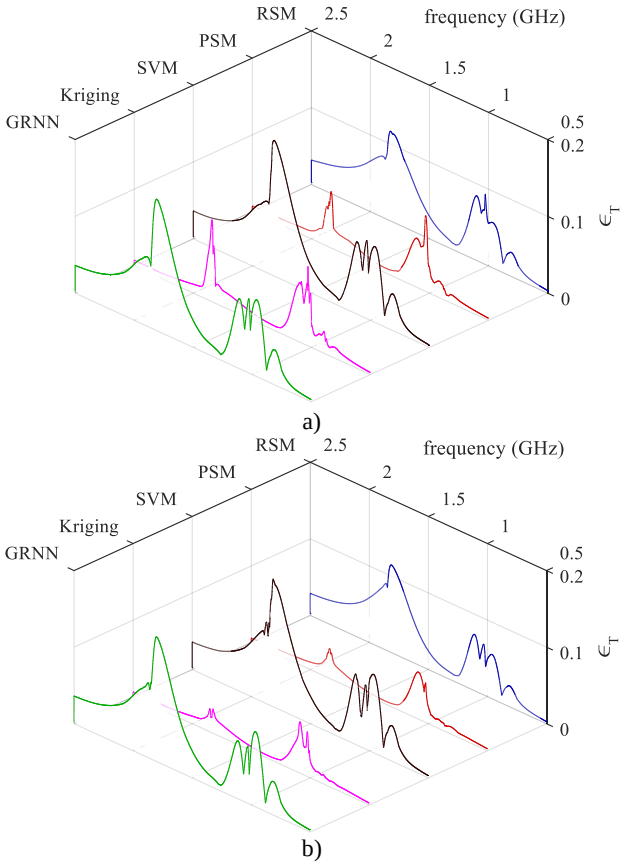

Fig. 11. Maximum testing errors for $|S_{11}|$ of the PIFA antenna using a uniform testing base point distribution with K = 3 and using: a) a star distribution of learning base points ($2n$ = 6); b) a box distribution of learning base points (2^n = 8).

TABLE II
PIFA ANTENNA SURROGATE MODELS PERFORMANCE FOR $|S_{11}|$

model	star distribution		box distribution	
	ϵ_{Tmax}	ϵ_{Lmax}	ϵ_{Tmax}	ϵ_{Lmax}
RSM	0.116770	0.080603	0.114430	0.107880
PSM	0.098251	0.054615	0.061406	0.013724
SVM	0.176450	0.077729	0.166740	0.166740
Kriging	0.106600	0.022197	0.066893	0.013126
GRNN	0.170990	0.081205	0.162690	0.162690

surrogate models. Again, these results indicate that the proposed polynomial-based surrogate model achieves the best generalization performance.

C. Package Via-Stripline Interconnect

Finally, as a third example, consider the package via-stripline-via interconnect shown in Fig. 12 (similar to that one in [39]). The interconnect starts with a coaxial port in contact with a via pad, whose via connects the top and middle layers. In the middle layer there is a stripline. At the end of the stripline there is another via that goes up to the top layer and connects to the other coaxial port.

1) Design Parameters

The interconnection is implemented on an FR4 substrate with a relative dielectric permittivity ε_r = 3.34, a loss tangent tan (δ) = 0.018, and thickness $H_1 = H_2$ = 22.5 μm. The length and width of the stripline are l_{tr} = 3000 μm and W_{tr} = 21 μm,

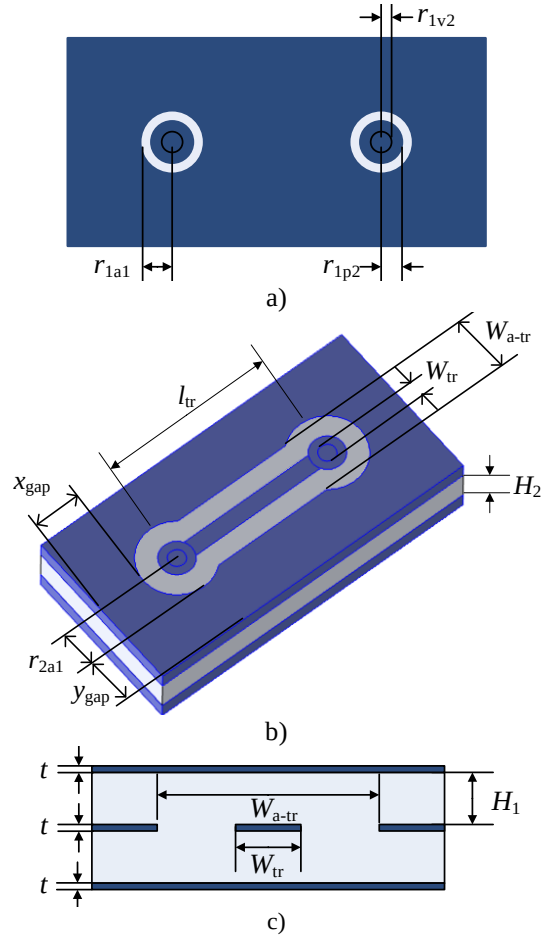

Fig. 12. Via-stripline package interconnect: a) 2D top view (top layer), b) middle layer 3D-model, and c) cross section.

respectively. Vias, pads and antipads radius are $r_{lv1} = r_{lv2}$ = 26 μm, $r_{2p1} = r_{1p1} = r_{2p2} = r_{1p2}$ = 54 μm, $r_{1a1} = r_{1a2}$ = 104 μm, $r_{2a1} = r_{2a2}$ = 220 μm. Distances from the interconnect to lateral and front walls are $x_{gap} = y_{gap}$ = 280 μm, respectively. Lossless metals with thickness t = 15 μm are used (thick metals).

The structure is implemented in COMSOL by using the simulation bounding box dimensions, boundary conditions, coaxial ports, and the meshing scheme proposed in [39]. We use a relatively coarse resolution discretization, such that each frequency sweep takes approximately 3 min.

2) Surrogate Model Implementation

For developing the surrogate model of the interconnect we use as input parameters the pads radius with $r_{1p} = r_{1p1} = r_{1p2}$. Then, $x = r_{1p}$. We use as a reference design $x^{(0)}$ = 54 (μm) over a region defined by τ = ± 5%. The EM response of the interconnect at $x^{(0)}$ is shown in Fig. 13.

To measure the generalization performance of the resultant polynomial surrogate model we use a uniform distribution with K = 10. Since this is a one-design variable example, star and box distribution yields to the same 2 learning base points, corresponding to the limits of the modeling region.

The maximum absolute testing errors as well as the order of the polynomial implemented at each simulated frequency point are shown in Fig. 14. Notice that a polynomial order higher than 2 is not required.

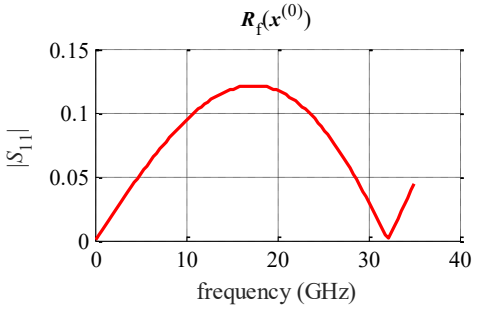

Fig. 13. EM response of the via-stripline interconnect at reference design $\boldsymbol{x}^{(0)}$.

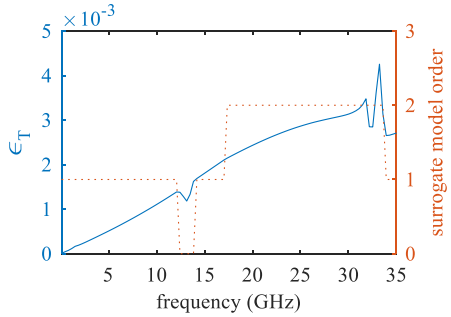

Fig. 14. Surrogate model maximum absolute testing error (solid line) and polynomial order (dotted line) at each simulated frequency point for the via-stripline package interconnect example.

The EM responses of the surrogate model at some testing base points are shown in Fig. 15. As in the previous examples, a very good match is obtained between the fine and the surrogate model responses at the testing base points.

3) Performance Comparison

Performance comparison for the five implemented surrogate models is illustrated in Fig. 16. Numerically, Table III shows the largest maximum absolute learning and testing errors for each implemented surrogate model. Once again, the results confirm that the polynomial surrogate model achieves the best generalization performance.

V. Discussion on the Modeling Region Size and Potential Applications

In all the previous examples (five different cases in total), we consider a relatively small modeling region size, using symmetric deviations of 5% for each design variable. The corresponding results for the surrogate models show that the proposed PSM exhibits the best performance, according to the generalization error, in all the five cases. We also implemented these examples using larger regions, with deviations of ±10% and ±15% for each design variable. The corresponding numerical results are in Tables IV to IX. It is seen that when using deviations of ±10%, the proposed PSM has the best performance in 4 out of the 5 cases, while when using deviations of ±15%, PSM shows the best performance in 3 out of the 5 cases. In those cases where PSM does not have the best performance, it still shows a very competitive behavior with respect to the surrogate modeling technique with best performance, which turned out different for each case. We have observed this same general trend when using even larger regions, finding that, when using a large modeling region size combined with a small number of learning base points, none of these surrogate modeling approaches consistently exhibits the best performance.

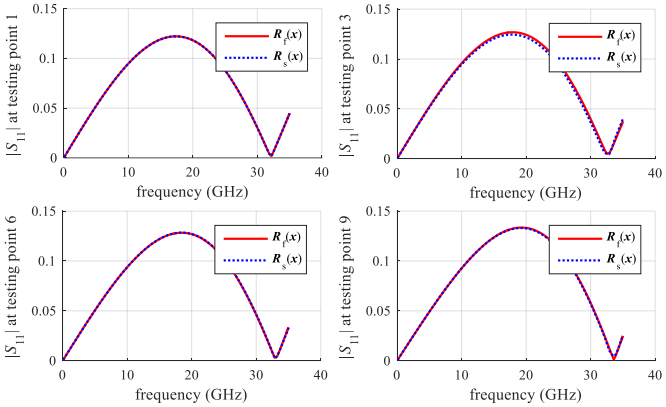

Fig. 15. Comparison between EM model and polynomial surrogate model responses at some testing base points for the via-stripline package interconnect.

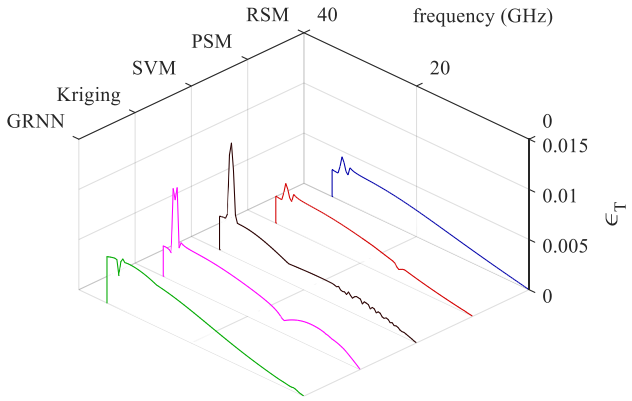

Fig. 16. Max. testing errors for $|S_{11}|$ of the via-stripline package interconnect using a uniform testing base point distribution with $K = 10$.

TABLE III
Package Interconnect Surrogate Model Performance for $|S_{11}|$

model	ϵ_{Tmax}	ϵ_{Lmax}
RSM	0.004435	3.15E-16
PSM	0.004435	0.001623
SVM	0.011196	0.010852
Kriging	0.009493	0.009354
GRNN	0.005134	0.000146

Our PSM technique can be useful for statistical analysis and yield estimations of RF and microwave circuits. A reliable Monte Carlo yield prediction requires a very high number of EM fine simulations to cover the entire statistics of possible outcomes [40]. To reduce this high computational cost, a PSM could be developed around the nominal design considering typical parameter tolerances due to the manufacturing process variability, which are usually small. Then, the statistical analysis could be realized directly on the PSM surrogate model, which is computationally cheap to develop, extremely fast to evaluate, and accurate for a small design region.

Our PSM methodology could also be used for design optimization of RF and microwave circuits. At each iteration, a

TABLE IV
SIW INTERCONNECT SURROGATE MODELS PERFORMANCE FOR $|S_{21}|$ USING $\tau = \pm$ [10% 10%]

model	star distribution		box distribution	
	ϵ_{Tmax}	ϵ_{Lmax}	ϵ_{Tmax}	ϵ_{Lmax}
RSM	0.24860	0.59749	0.29747	0.11562
PSM	0.18947	0.09072	0.28674	0.13234
SVM	0.40140	0.28565	0.18779	0.12682
Kriging	0.41565	0.26696	0.35191	0.20865
GRNN	0.32309	0	0.46267	0

TABLE V
PIFA ANTENNA SURROGATE MODELS PERFORMANCE FOR $|S_{11}|$ USING $\tau = \pm$ [10% 10% 10% 10%]

model	star distribution		box distribution	
	ϵ_{Tmax}	ϵ_{Lmax}	ϵ_{Tmax}	ϵ_{Lmax}
RSM	0.31910	0.62052	0.27920	0.13024
PSM	0.22117	0.11758	0.10447	0.03437
SVM	0.40407	0.14461	0.34050	0.34050
Kriging	0.28935	0.01368	0.14167	0.04073
GRNN	0.38304	0.14887	0.33434	0.33434

TABLE VI
PACKAGE INTERCONNECT SURROGATE MODEL PERFORMANCE FOR $|S_{11}|$ USING $\tau = \pm$ 10%

model	ϵ_{Tmax}	ϵ_{Lmax}
RSM	0.01062	7.00E-16
PSM	0.01062	0.00569
SVM	0.02667	0.02775
Kriging	0.02592	0.02132
GRNN	0.01655	9.81E-11

TABLE VII
SIW INTERCONNECT SURROGATE MODELS PERFORMANCE FOR $|S_{21}|$ USING $\tau = \pm$ [15% 15%]

model	star distribution		box distribution	
	ϵ_{Tmax}	ϵ_{Lmax}	ϵ_{Tmax}	ϵ_{Lmax}
RSM	0.33525	0.36726	0.25224	0.10316
PSM	0.22262	0.16685	0.23369	0.11208
SVM	0.47614	0.34309	0.17508	0.22701
Kriging	0.49633	0.31750	0.36596	0.36596
GRNN	0.57570	0	0.56991	0

TABLE VIII
PIFA ANTENNA SURROGATE MODELS PERFORMANCE FOR $|S_{11}|$ USING $\tau = \pm$ [15% 15% 15% 15%]

model	star distribution		box distribution	
	ϵ_{Tmax}	ϵ_{Lmax}	ϵ_{Tmax}	ϵ_{Lmax}
RSM	0.49730	0.76730	0.42275	0.65000
PSM	0.35426	0.17725	0.20638	0.05851
SVM	0.55584	0.22893	0.45227	0.45227
Kriging	0.40881	0.02462	0.26068	0.06449
GRNN	0.51803	0.23650	0.42510	0.42510

PSM model with a reduced number of learning base points around the current iterate can be obtained on a relatively small region; the optimal solution of the current PSM model would yield the next iterate, around which a new PSM model can be obtained, etc. This approach should require a smaller number of EM fine model simulations than that one required by direct EM optimization.

A third potential application for the proposed PSM methodology consists of using it to build mathematical maps between coarse and fine model design variables, for input space mapping approaches [41]. Since the relationship between fine and coarse model variables is usually not too complex [42], the use of low-order polynomial surrogates is appropriate to represent it. This application is currently being developed by the authors.

TABLE IX
PACKAGE INTERCONNECT SURROGATE MODEL PERFORMANCE FOR $|S_{11}|$ USING $\tau = \pm$ 15%

model	ϵ_{Tmax}	ϵ_{Lmax}
RSM	0.01305	0.01043
PSM	0.01409	0.01348
SVM	0.03747	0.05000
Kriging	0.00746	0.00357
GRNN	0.00601	0.00202

VI. CONCLUSIONS

We presented a general formulation for a polynomial surrogate modeling (PSM) approach exploiting the multinomial theorem. Some features of our proposal are: a) the polynomial is expanded using the multinomial theorem, which includes all cross terms and avoids redundant terms; b) globally optimal weighting factors are calculated in closed form using two different approaches, automatically selecting one of them according to the best conditioned system; c) a minimum number of learning base points is not required for developing the surrogate model; and d) the order of the polynomial can be different at each simulated frequency point, according to the local generalization performance.

Our PSM methodology was compared with four surrogate modeling techniques: response surface methodology, support vector machines, generalized regression neural networks and Kriging; by modeling three microwave structures. Our proposal showed the best performance when the size of the region of interest is small, and a very good performance for larger regions, in spite of its simplicity of formulation and implementation. Our PSM methodology proves to be an excellent candidate for developing EM surrogate models when the amount of base points is very limited and the size of the region of interest is relatively small.

REFERENCES

[1] A. J. Booker, J. E. Dennis Jr., P. D. Frank, D. B. Serafini, V. Torczon, and M. W. Trosset, "A rigorous framework for optimization of expensive functions by surrogates," *Structural Optimization*, vol. 17, no. 1, pp. 1-13, Feb. 1999.

[2] M. B. Yelten, T. Zhu, S. Koziel, P. D. Franzon, and M. B. Steer, "Demystifying surrogate modeling for circuits and systems," *IEEE Circuits and Systems Magazine*, vol. 12, no. 1, pp. 45-63, First Quarter 2012.

[3] S. Koziel and X. S. Yang, *Computational Optimization, Methods and Algorithms.* vol. 356. Berlin, BE: Springer, 2011.

[4] J. C. Cervantes-González, J. E. Rayas-Sánchez, C. A. López, J. R. Camacho-Pérez, Z. Brito-Brito, and J. L. Chavez-Hurtado, "Space mapping optimization of handset antennas considering EM effects of mobile phone components and human body," *Int. J. RF and Microwave CAE*, vol. 26, no. 2, pp. 121-128, Feb. 2016.

[5] S. Koziel and L. Leifsson, *Surrogate-Based Modeling and Optimization: Applications in Engineering*, New York, NY: Springer,

2013.
[6] M. C. Fu, *Handbook of Simulation Optimization.* vol. 216. New York, NY: Springer, 2014.
[7] M. Redhe and L. Nilsson, "Optimization of the new Saab 9-3 exposed to impact load using a space mapping technique," *Structural and Multidisciplinary Optimization*, vol. 27, no. 5, pp. 411-420, Jul. 2004.
[8] J. Zhang and D. Zhang, "Study of response surface methodology in thermal optimization design of multichip modules," *Trans. on Components, Packaging and Manufacturing Technology*, vol. 3, no. 12, pp. 2075-2080, Dec. 2013.
[9] D. M. Osborne, R. L. Armacost, and J. Pet-Edwards, "State of the art in multiple response surface methodology," in *IEEE Int. Conf. on Systems, Man, and Cybernetics*, Florida, USA, Oct. 1997, vol. 4, pp. 3833-3838.
[10] T. Mandic, R. Gillon, and A. Baric, "IC-Stripline design optimization using response surface methodology," in *9th Int. Workshop on Electromagnetic Compatibility of Integrated Circuits (EMC Compo 2013)*, Nara, Japan, Dec. 2013, pp. 69-73.
[11] M. Mussetta, D. Caputo, A. Pirisi, F. Grimaccia, L. Valbonesi, and R. E. Zich, "Neural networks and evolutionary algorithm application to complex EM structures modeling," in *Int. Conf. on Electromagnetics in Advanced Applications (ICEAA 2009)*, Sept. 2009, pp. 1020-1023.
[12] S. Haykin, *Neural Networks. A Comprehensive Foundation.* USA: Prentice Hall, 1999.
[13] J. E. Rayas-Sánchez, "EM-based optimization of microwave circuits using artificial neural networks: the state-of-the-art*," IEEE Trans. Microwave Theory Techn.*, vol. 52, no. 1, pp. 420-435, Jan. 2004.
[14] Z. Raida, "Modeling EM structures in the neural network toolbox of MATLAB," *IEEE Antennas and Propagation Magazine*, vol. 44, no. 6, pp. 46-67, Dec. 2002.
[15] P. Mahouti, F. Günes, S. Demirel, A. Uluslu, and M. A. Belen, "Efficient scattering parameter modeling of a microwave transistor using generalized regression neural network," in *IEEE Int. Conf. on Microwaves, Radar, and Wireless Communication (MIKON 2014)*, Poland, Jun. 2014, pp. 1-4.
[16] D. F. Specht, "A general regression neural network," *IEEE Trans. on Neural Networks*, vol. 2, no. 6, pp. 568-576, 1991.
[17] B. N. Panda, M. V. A. R. Bahubalendruni, and B. B. Biswal, "Optimization of resistance spot welding parameters using differential evolution algorithm and GRNN," in *IEEE Int. Conf. on Intelligent Systems and Control (ISCO 2014)*, vol. 2, no. 6, India, Jan. 2014, pp. 50-55.
[18] Q. J. Zhang and K. C. Gupta, *Neural Networks for RF and Microwave Design*. Norwood, MA: Artech House, 2000.
[19] H. Li-Na and N. Jing-Chang, "Researches on GRNN neural network in RF nonlinear systems modeling," in *IEEE Int. Conf. on Computational Problem-Solving (ICCP 2011)*, Romania, Aug. 2011, pp. 1-4.
[20] G. Angiulli, M. Cacciola, and M. Versaci, "Microwave devices and antennas modelling by support vector regression machines," *IEEE Trans. on Magnetics*, vol. 43, no. 4, pp. 1589-1592, 2007.
[21] L. Xia, J. Meng, R. Xu, B. Yan, and Y. Guo, "Modeling of 3-D vertical interconnect using support vector machine regression," *IEEE Microwave and Wireless Components Letters*, vol. 16, no. 12, pp. 639-641, 2006.
[22] N. T. Tokan and F. Günes, "Knowledge-based support vector synthesis of the microstrip lines," *Progress in Electromagnetics Research*, vol. 92, pp. 65-77, 2009.
[23] S. Demirel, F. Günes, and A. K. Keskin, "Design of an ultrawide band low noise microstrip amplifier using 3D Sonnet-based SVRM with particle swarm optimization for space applications," in *IEEE Int. Conf. on Recent Advances in Space Technologies (RAST)*, Istanbul, Turkey, Jun. 2013, pp. 445-450.
[24] N. T. Tokan and F. Günes, "Analysis and synthesis of the microstrip lines based on support vector regression," in *IEEE European Microwave Conf. (EuMC 2008)*, Amsterdam, Netherlands, Oct. 2008, pp. 1473-1476.
[25] J. P. Jacobs, "Bayesian support vector regression with automatic relevance determination kernel for modeling of antenna input characteristics," *IEEE Trans. on Antennas and Propagation*, vol. 60, no. 4, pp. 2114-2118, 2012.
[26] X. Ren and T. Kazmierski, "Performance modelling and optimization of RF circuits using support vector machines," in *Int. Conf. on Mixed Design (MIXDES 2007)*, Poland, Jun. 2007, pp. 317-321.
[27] W. C. M. Van Beers, "Kriging metamodeling in discrete-event simulation: an overview," in *Winter Simulation Conf.*, Dec. 2005, pp. 4-7.
[28] W. C. M. van Beers and J. P. C. Keijnen, "Kriging interpolation in simulation: a survey," in *Winter Simulation Conf.*, Dec. 2004, pp. 5-8.
[29] B. Xia, Z. Ren, and C. S. Koh, "Selecting proper kriging surrogate model for optimal design of electromagnetic problem," in *9th IET Int. Conf. on Computation in Electromagnetics*, London, UK, Mar., 2014, pp. 1-4.
[30] I. Couckuyt, S. Koziel, and T. Dhane, "Surrogate modeling of microwave structures using Kriging, co-kriging and space mapping," *Int. J. Numerical Modelling: Electron. Networks, Dev. Fields*., vol. 26, no. 1, pp. 64-73, 2013.
[31] S. Koziel and J. W. Bandler, "Accurate modeling of microwave devices using kriging-corrected space mapping surrogates," *Int. J. Numerical Modelling: Electron. Networks, Dev. Fields*., vol. 25, no. 1, pp. 1-14, 2012.
[32] J. E. Rayas-Sánchez, J. L. Chavez-Hurtado, and Z. Brito-Brito, "Design optimization of full-wave EM models by low-order low-dimension polynomial surrogate functionals," *Int. J. Numerical Modelling: Electron. Networks, Dev. Fields*., published online: 13 Sep. 2015, regular publication pending.
[33] J. E. Rayas-Sánchez, J. L. Chávez-Hurtado, and Z. Brito-Brito, "Enhanced formulation for polynomial-based surrogate modeling of microwave structures in frequency domain," in *IEEE MTT-S Int. Conf. Num. EM Mutiphysics Modeling Opt. RF, Microw., Terahertz App. (NEMO-2015)*, Ottawa, ON, Aug. 2015, pp. 1-3.
[34] J. L. Chávez-Hurtado and J. E. Rayas-Sánchez, "Polynomial-based surrogate modeling of microwave structures in frequency domain exploiting the multinomial theorem," in *IEEE MTT-S Int. Microwave Symp. Dig.*, San Francisco, CA, May 2016, pp. 1-3.
[35] S. Ogurtsov, S. Koziel, and J. E. Rayas-Sánchez, "Design optimization of a broadband microstrip-to-SIW transition using surrogate modeling and adaptive design specifications," in *Int. Review of Progress in Applied Computational Electromagnetics (ACES 2010)*, Tampere, Finland, Apr. 2010, pp. 878-883.
[36] Z. Brito-Brito, J. E. Rayas-Sánchez, J. C. Cervantes-González, and C. A. López, "Impact of 3D EM model configuration on the direct optimization of microstrip structures," in *COMSOL Conf.*, Boston, MA, Oct. 2013, pp. 1-5.
[37] J. L. Chavez-Hurtado, J. E. Rayas-Sánchez, and Z. Brito-Brito, "Reliable full-wave EM simulation of a single-layer SIW interconnect with transitions to microstrip lines," in *COMSOL Conf.*, Boston, MA, Oct. 2014, pp. 1-5.
[38] J. C. Cervantes-González, J. E. Rayas-Sánchez, C. A. López, J. R. Camacho-Pérez, Z. Brito-Brito, and J. L. Chavez-Hurtado, "Space mapping optimization of handset antennas considering EM effects of mobile phone components and human body," *Int. J. RF and Microwave CAE*, vol. 26, no. 2, pp. 121-128, Feb. 2016.
[39] J. C. Cervantes-González, C. A. López, J. E. Rayas-Sánchez, Z. Brito-Brito, and G. Hernández-Sosa, "Return-loss minimization of package interconnects through input space mapping using FEM-based models," in *Proc. SBMO/IEEE MTT-S Int. Microwave Optoelectronics Conf. (IMOC-2013)*, Rio de Janeiro, Brazil, Aug. 2013, pp. 1-4.
[40] J. E. Rayas-Sánchez and V. Gutiérrez-Ayala, "EM-based Monte Carlo analysis and yield prediction of microwave circuits using liner-input neural-output space mapping*," IEEE Trans. Microwave Theory Techn.*, vol. 54, no. 12, pp. 4528-4537, Jan. 2006.
[41] J. W. Bandler, Q. Cheng, S. A. Dakroury, A. S. Mohamed, M. H. Bakr, K. Madsen, and J. Søndergaard, "Space mapping: the state of the art," *IEEE Trans. Microwave Theory Techn.*, vol. 52, no. 1, pp. 337-361, Jan. 2004.
[42] J. E. Rayas-Sanchez, "Power in simplicity with ASM: tracing the aggressive space mapping algorithm over two decades of development and engineering applications," *IEEE Microwave Magazine*, vol. 17, no. 4, pp. 64-76, Apr. 2016.

José Luis Chávez-Hurtado was born in Guadalajara, Mexico, in 1985. He received the B.Sc. and M.Sc. degrees in electronics engineering from ITESO - the Jesuit University of Guadalajara, Mexico, in 2007 and 2009, respectively. He also received the Master's degree in business and economics from the University of Guadalajara, Mexico, in 2012. He is currently working towards the Ph.D. degree in engineering sciences at the Department of Electronics, Systems, and Informatics, ITESO.

Since 2012, he has been an adjunct professor with the Mathematics Department, University of Guadalajara – Business School, Mexico. Since 2014, he has also been an adjunct professor with the Department of Electronics, Systems, and Informatics, ITESO – The Jesuit University of Guadalajara, Mexico. His research interests include optimization methods for modeling and design of microwave circuits, surrogate-based optimization, neural network applications, linear programming and nonlinear forecasting.

José Ernesto Rayas-Sánchez received the B.Sc. degree in electronics engineering from ITESO, Guadalajara, Mexico, the Masters degree in electrical engineering from Monterrey Tec, Monterrey, Mexico, and the Ph.D. degree in electrical engineering from McMaster University, Ontario, Canada. He is *Profesor Numerario* (honorary distinction) with ITESO – The Jesuit University of Guadalajara, where he is Chair of the Doctoral Program in Engineering Sciences. He currently leads the Research Group on Computer-Aided Engineering of Circuits and Systems (CAECAS) at ITESO. His research focuses on computer-aided and knowledge-based modeling, design and optimization of high-frequency electronic circuits and devices (including RF, microwave and wireless circuits).

Dr. Rayas-Sánchez is Vice-Chair of the Technical Committee on Computer Aided Design (MTT-1) of the IEEE Microwave Theory and Techniques Society (MTT-S). He is member of the Technical Program Reviewers Committee of the IEEE MTT-S International Microwave Symposium (IMS). He serves as reviewer for the following publications: IEEE Transactions on Microwave Theory and Techniques, IEEE Microwave and Wireless Components Letters, IEEE Antennas and Wireless Propagation Letters, IET Microwaves, Antennas & Propagation Journal, International Journal of RF and Microwave Computer-Aided Engineering (Wiley InterScience), and IEEE Latin America Transactions. He was the General Chair of the First IEEE MTT-S Int. Microwave Workshop Series in Region 9 (IMWS2009-R9) on Signal Integrity and High-Speed Interconnects (Guadalajara, Mexico, Feb. 2009). During 2004 and 2005, he was the IEEE Mexican Council Chair, as well as the IEEE Region 9 Treasurer. Since 2013, he is IEEE MTT-S Regional Coordinator for Latin America. He currently is the General Chair of the First IEEE MTT-S Latin America Microwave Conference (LAMC-2016, Puerto Vallarta, Mexico, Dec. 2016).